Supporting Information

Designing asymmetric Dy_2 single-molecule magnets with two-step relaxation processes by the modification of the coordination environments of Dy(III) ions

Yuan Huang,[a] Jia-Xin Li,[b] Yu Ge,[a] Xia-Mei Zhang,[a] Yang Xu,[a] Yahong Li,*[a] Yi-Quan Zhang,*[b] and Jin-Lei Yao*[c]

[a]*College of Chemistry, Chemical Engineering and Materials Science, Soochow University, Suzhou 215123, P. R. China. E-mail: liyahong@suda.edu.cn*

[b]*Jiangsu Key Laboratory for NSLSCS, School of Physical Science and Technology, Nanjing Normal University, Nanjing 210023, P. R. China. E-mail: zhangyiquan@njnu.edu.cn*

[c]*Jiangsu Key Laboratory of Micro and Nano Heat Fluid Flow Technology and Energy Application, School of Mathematics and Physics, Suzhou University of Science and Technology, Suzhou 215009, P. R. China. E-mail: jlyao@usts.edu.cn*

Content

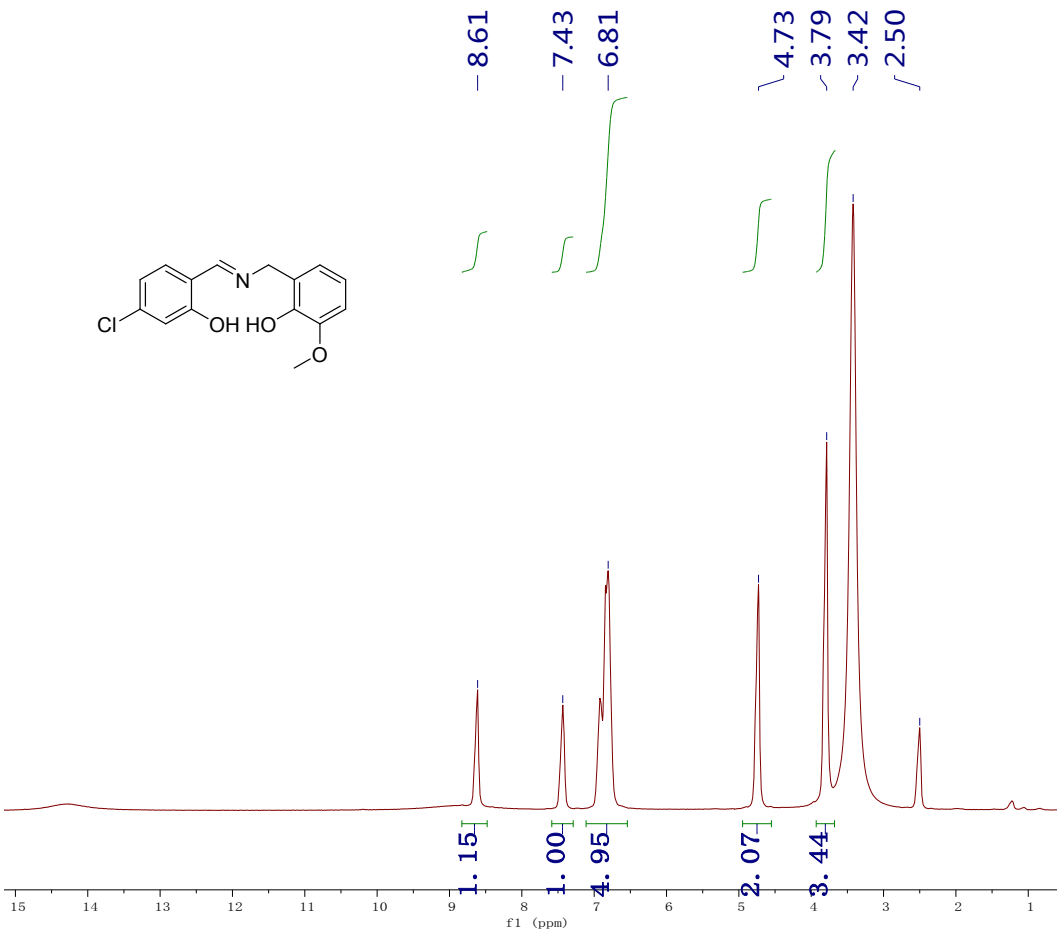

Fig. S1 The ^{1}H NMR spectrum (DMSO-d_6) of the H_2L ligand.

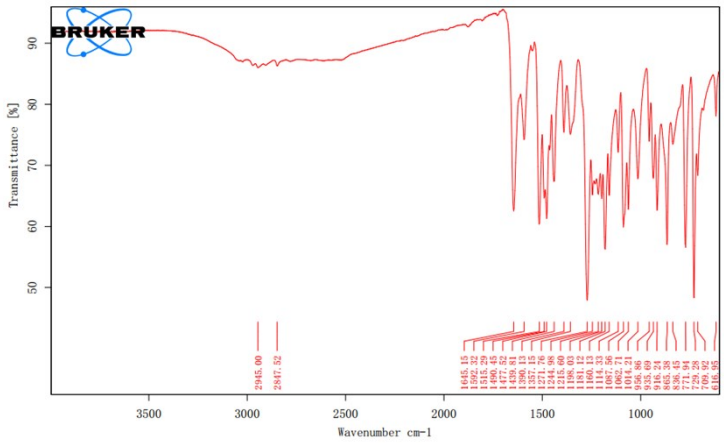

(a)

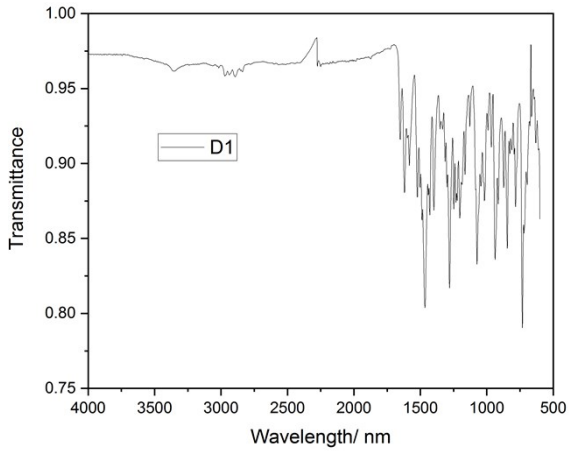

(b)

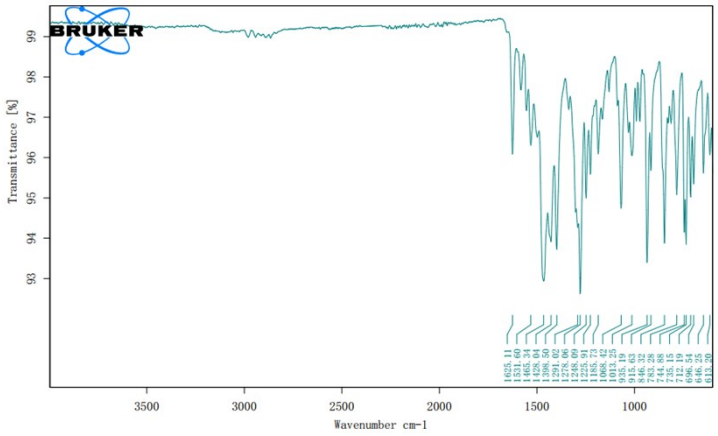

(c)

Fig. S2 The IR spectra of the (a) ligand, (b) complex **1** and (c) complex **2**.

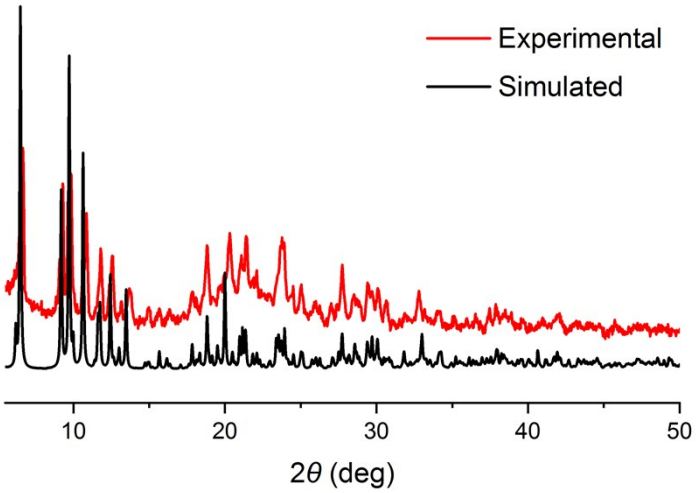

(a)

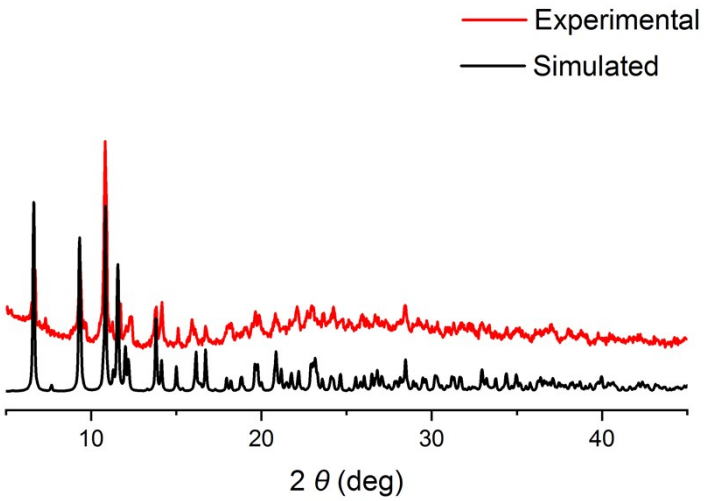

(b)

Fig. S3 The PXRD patterns of (a) complex **1** and (b) complex **2**.

Table S1 Selected bond lengths (Å) and angle (°) for complex **1**

Bond length (Å)		Bond angle (°)					
Dy1-Dy2	3.7830(3)	O1-Dy1-Dy2	169.00(7)	O7-Dy1-O11	154.97(9)	O5-Dy2-Dy1	88.46(7)
Dy1-O1	2.181(3)	O1-Dy1-O2	145.06(9)	O7-Dy1-N1	80.50(9)	O5-Dy2-O2	80.94(9)
Dy1-O2	2.344(2)	O1-Dy1-O3	144.30(9)	O9-Dy1-Dy2	75.11(7)	O5-Dy2-O3	85.30(10)
Dy1-O3	2.272(2)	O1-Dy1-O7	92.14(10)	O9-Dy1-O10	72.11(9)	O5-Dy2-O4	65.74(9)
Dy1-O7	2.273(3)	O1-Dy1-O9	94.13(10)	O9-Dy1-O11	50.75(9)	O5-Dy2-O8	131.24(9)
Dy1-O9	2.452(3)	O1-Dy1-O10	78.97(9)	O9-Dy1-N1	125.54(9)	O5-Dy2-O12	152.66(10)
Dy1-O10	2.483(3)	O1-Dy1-O11	77.07(10)	O10-Dy1-Dy2	99.42(6)	O5-Dy2-N2	78.19(11)
Dy1-O11	2.576(3)	O1-Dy1-N1	74.84(10)	O10-Dy1-O11	114.89(9)	O6-Dy2-Dy1	153.68(9)
Dy1-N1	2.511(3)	O2-Dy1-Dy2	36.27(6)	O10-Dy1-N1	149.07(9)	O6-Dy2-O2	145.61(10)
Dy2-O2	2.346(2)	O2-Dy1-O9	79.45(9)	O11-Dy1-Dy2	94.02(7)	O6-Dy2-O3	136.53(10)
Dy2-O3	2.327(2)	O2-Dy1-O10	66.33(9)	N1-Dy1-Dy2	109.37(7)	O6-Dy2-O4	78.04(11)
Dy2-O4	2.500(3)	O2-Dy1-O11	120.55(9)	N1-Dy1-O11	74.92(9)	O6-Dy2-O5	117.46(11)
Dy2-O5	2.253(3)	O2-Dy1-N1	136.25(9)	O2-Dy2-Dy1	36.23(6)	O6-Dy2-O8	74.81(10)
Dy2-O6	2.190(3)	O3-Dy1-Dy2	35.14(6)	O2-Dy2-O4	135.76(9)	O6-Dy2-O12	78.96(11)
Dy2-O8	2.609(3)	O3-Dy1-O2	70.24(9)	O2-Dy2-O8	116.32(9)	O6-Dy2-N2	75.07(11)
Dy2-O12	2.443(3)	O3-Dy1-O7	102.09(9)	O2-Dy2-O12	74.64(10)	O8-Dy2-Dy1	84.70(6)
Dy2-N2	2.437(3)	O3-Dy1-O9	87.25(9)	O2-Dy2-N2	81.48(10)	O12-Dy2-Dy1	79.14(7)
		O3-Dy1-O10	134.42(9)	O3-Dy2-Dy1	34.19(6)	O12-Dy2-O4	141.55(10)
		O3-Dy1-O11	76.41(9)	O3-Dy2-O2	69.28(8)	O12-Dy2-O8	72.18(10)
		O3-Dy1-N1	75.48(9)	O3-Dy2-O4	79.37(9)	N2-Dy2-Dy1	117.70(8)
		O7-Dy1-Dy2	98.54(6)	O3-Dy2-O8	63.09(9)	N2-Dy2-O4	116.70(11)
		O7-Dy1-O2	80.96(9)	O3-Dy2-O12	97.18(10)	N2-Dy2-O8	145.61(10)
		O7-Dy1-O9	153.94(9)	O3-Dy2-N2	148.34(10)	N2-Dy2-O12	86.12(12)
		O7-Dy1-O10	84.36(10)	O4-Dy2-Dy1	111.57(7)	Dy1-O2-Dy2	107.50(10)
				O4-Dy2-O8	72.28(9)	Dy1-O3-Dy2	110.67(10)

Table S2 Selected bond lengths (Å) and angle (°) for complex **2**

Bond length (Å)		Bond angle (°)			
Dy1-O1	2.327(2)	O1-Dy1-O2	82.35(8)	O1-Dy2-O3	71.11(7)
Dy1-O2	2.466(2)	O1-Dy1-O3	69.78(7)	O1-Dy2-O5	133.45(7)
Dy1-O3	2.370(2)	O1-Dy1-O6	66.26(7)	O1-Dy2-O7	81.12(8)
Dy1-O6	2.499(2)	O1-Dy1O11	80.62(8)	O1-Dy2-N1	76.52(8)
Dy1-O8	2.185(2)	O1-Dy1-N2	142.00(8)	O3-Dy2-O5	67.08(7)
Dy1-O9	2.310(2)	O2-Dy1-O6	118.80(8)	O3-Dy2-N1	139.90(8)
Dy1-O11	2.483(2)	O2-Dy1-O11	51.49(8)	O4-Dy2-O1	141.48(8)
Dy1-N2	2.454(3)	O3-Dy1O2	81.72(8)	O4-Dy2-O3	144.84(8)
Dy2-O1	2.295(2)	O3-Dy1-O6	127.14(8)	O4-Dy2-O5	77.79(8)
Dy2-O3	2.326(2)	O3-Dy1-O11	127.59(8)	O4-Dy2-O7	87.51(9)
Dy2-O4	2.197(2)	O3-Dy1-N2	76.83(8)	O4-Dy2-N1	73.97(9)
Dy2-O5	2.484(2)	O8-Dy1-O1	143.28(8)	O4-Dy2-O12	91.56(10)
Dy2-O7	2.311(2)	O8-Dy1-O2	109.44(9)	O7-Dy2-O3	85.92(8)
Dy2-N1	2.479(3)	O8-Dy1-O3	144.63(8)	O7-Dy2-O5	76.49(9)
Dy2-O12	2.239(3)	O8-Dy1-O6	77.94(8)	O7-Dy2-N1	112.00(9)
		O8-Dy1-O9	87.76(9)	N1-Dy2-O5	149.92(8)
		O8-Dy1-O11	80.72(9)	O12-Dy2-O1	111.09(10)
		O8-Dy1-N2	74.10(8)	O12-Dy2-O3	83.30(9)
		O9-Dy1-O1	90.45(8)	O12-Dy2-O5	83.66(10)
		O9-Dy1-O2	159.48(8)	O12-Dy2-O7	159.87(11)
		O9-Dy1-O3	77.76(8)	O12-Dy2-N1	86.95(10)
		O9-Dy1-O6	74.77(9)	Dy2-O1-Dy1	106.96(8)
		O9-Dy1-O11	146.16(9)	C13-O1-Dy1	118.89(18)
		O9-Dy1-N2	99.88(9)	C13-O1-Dy2	125.35(18)
		O11-Dy1-O6	71.75(8)	N3-O2-Dy1	96.49(18)
		N2-Dy1-O2	75.27(8)	Dy2-O3-Dy1	104.55(8)
		N2-Dy1-O6	151.74(8)	N3-O11-Dy1	96.01(18)
		N2-Dy1-O11	107.22(9)		

SHAPE program details for 1 and 2

Table S3 Agreement factors between the coordination polyhedron of the Dy^{III} ions in eight-coordinated and the various ideal polyhedral calculated by the SHAPE program

	SAPR-8(D_{4d})	TDD-8(D_{2d})
1_Dy1	3.072	1.825
1_Dy2	1.227	2.200
2_Dy1	3.073	2.098

Table S4 Agreement factors between the coordination polyhedron of the Dy^{III} ion in seven-coordinated and the various ideal polyhedral calculated by the SHAPE program

	PBPY-7(D_{5h})	CTPR-7(C_{2v})
2_Dy2	2.429	1.885

(a)

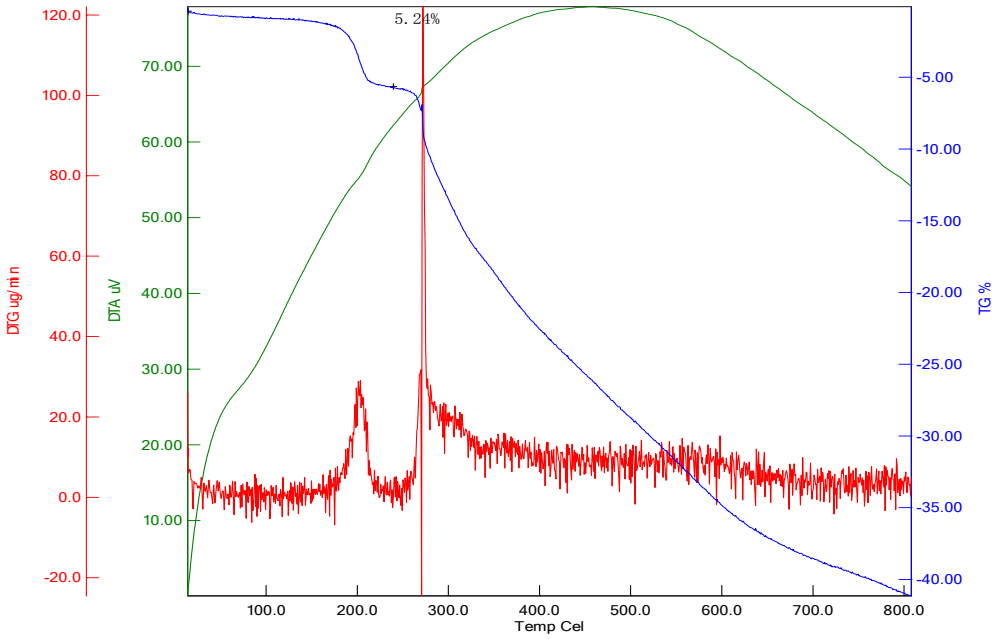

(b)

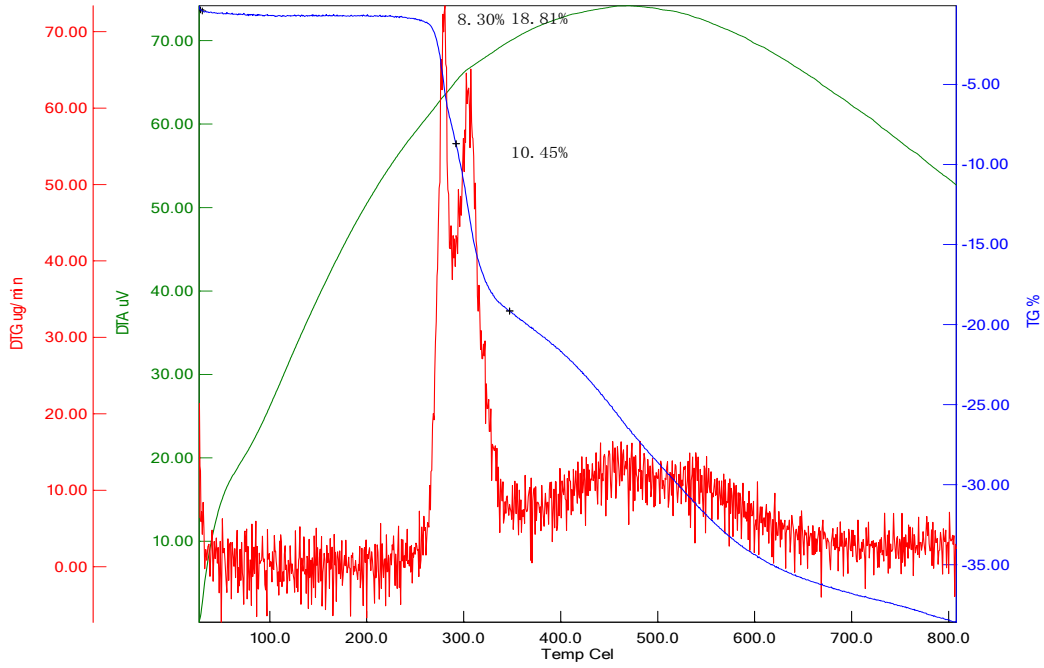

Fig. S4 The TGA curves of (a) complex **1** and (b) complex **2**.

Table S5 Relaxation fitting parameters from Least-Squares Fitting of $\chi(\omega)$ data for **1**

T (K)	$\chi_{S,tot}$ (cm^3mol^{-1})	$\Delta\chi_1$ (cm^3mol^{-1})	$\Delta\chi_2$ (cm^3mol^{-1})	α_1	α_2	τ_1 (s)	τ_2 (s)
8	6.55E-05	1.29E+00	1.12E+00	1.31E-16	8.65E-02	2.81E-02	1.85E-03
9	7.35E-05	1.42E+00	1.05E+00	1.21E-16	7.99E-02	2.45E-02	1.05E-03
10	1.88E-05	1.22E+00	9.50E-01	1.50E-16	7.57E-02	1.52E-02	5.76E-04
11	3.72E-05	1.08E+00	8.69E-01	3.37E-16	7.51E-02	9.97E-03	3.12E-04
12	5.74E-05	9.84E-01	8.04E-01	1.66E-16	7.73E-02	6.82E-03	1.63E-04
13	1.61E-04	8.97E-01	7.47E-01	2.77E-18	7.95E-02	4.76E-03	8.30E-05
14	3.51E-04	8.22E-01	7.00E-01	5.17E-18	9.03E-02	3.39E-03	4.20E-05
15	5.83E-04	7.57E-01	6.59E-01	5.34E-18	1.19E-01	2.44E-03	2.08E-05
16	6.58E-04	7.01E-01	6.23E-01	9.85E-18	1.49E-01	1.77E-03	1.04E-05
17	2.00E-17	6.50E-01	5.94E-01	2.16E-17	2.46E-01	1.28E-03	4.22E-06
18	3.42E-17	6.17E-01	5.56E-01	3.37E-17	3.25E-06	9.22E-04	5.53E-06
19	4.57E-17	5.77E-01	5.33E-01	5.50E-17	3.04E-06	6.56E-04	4.03E-06
20	4.60E-17	5.41E-01	5.13E-01	9.16E-17	3.38E-06	4.58E-04	3.22E-06
21	3.99E-17	5.04E-01	4.99E-01	1.36E-16	3.80E-06	3.11E-04	3.43E-06
22	7.91E-18	4.59E-01	4.99E-01	2.43E-16	2.94E-06	2.07E-04	5.06E-06
23	2.11E-19	3.90E-01	5.26E-01	3.63E-16	2.43E-06	1.37E-04	8.57E-06
24	5.89E-19	2.11E-01	6.67E-01	4.65E-16	4.50E-06	1.07E-04	1.66E-05

Table S6 Relaxation fitting parameters from Least-Squares Fitting of $\chi(\omega)$ data for **2**

T (K)	$\chi_{S,tot}$ (cm^3mol^{-1})	$\Delta\chi_1$ (cm^3mol^{-1})	$\Delta\chi_2$ (cm^3mol^{-1})	α_1	α_2	τ_1 (s)	τ_2 (s)
5	7.47E-02	1.20E+00	2.44E+00	8.97E-02	1.46E-02	9.36E-03	3.14E-02
6	7.64E-02	1.45E+00	3.22E+00	4.10E-02	3.07E-02	5.02E-03	5.83E-02
7	6.15E-02	1.33E+00	2.44E+00	5.91E-02	3.28E-02	2.63E-03	3.47E-02
8	5.93E-02	9.13E-01	2.78E+00	1.29E-02	1.95E-01	1.21E-03	2.55E-02
9	5.75E-02	9.38E-01	2.01E+00	4.44E-02	1.21E-01	6.80E-04	1.31E-02
10	5.47E-02	9.45E-01	1.59E+00	9.93E-02	7.05E-02	3.74E-04	7.72E-03
11	7.37E-07	1.01E+00	1.30E+00	2.23E-01	3.60E-02	1.77E-04	4.85E-03
12	5.22E-07	9.62E-01	1.14E+00	3.36E-01	3.08E-02	7.48E-05	3.04E-03
13	6.80E-07	9.05E-01	1.04E+00	4.37E-01	2.98E-02	2.88E-05	1.94E-03
14	6.23E-07	7.87E-01	1.02E+00	4.08E-01	4.03E-02	1.09E-05	1.26E-03
15	1.44E-06	7.20E-01	9.47E-01	3.27E-01	3.50E-02	7.50E-06	8.51E-04
16	3.04E-06	6.81E-01	8.74E-01	2.45E-01	2.74E-02	7.05E-06	5.98E-04
17	7.08E-07	6.74E-01	7.84E-01	2.07E-01	1.33E-02	7.84E-06	4.38E-04
18	2.09E-06	6.33E-01	7.45E-01	2.84E-15	1.13E-02	8.66E-06	3.17E-04
19	2.75E-12	6.45E-01	6.59E-01	8.26E-15	3.56E-03	1.12E-05	2.42E-04
20	6.63E-12	6.75E-01	5.63E-01	2.02E-15	2.55E-08	1.36E-05	1.86E-04

(a)

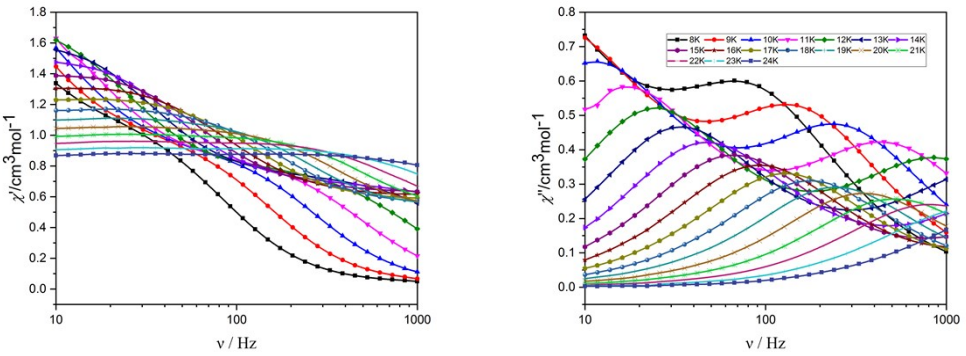

(b)

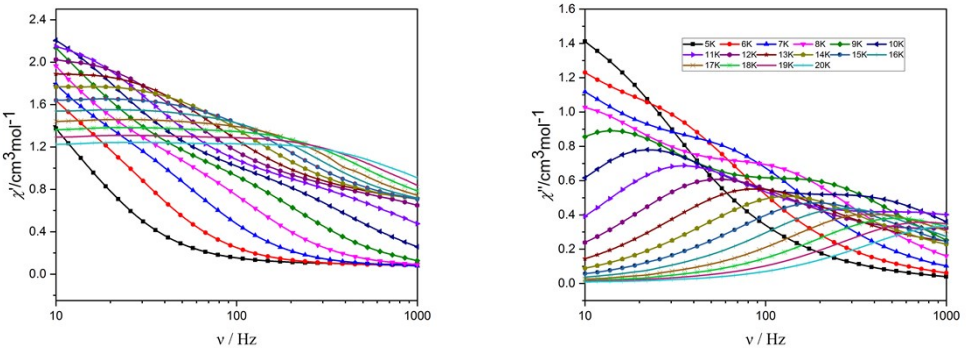

Fig. S5 Frequency dependence of the in-phase (χ') and out-of-phase (χ'') magnetic susceptibilities for complex **1** (a) in the range of 8 to 24 K and **2** (b) in the range of 5 to 20 K under zero *dc* field.

(a)

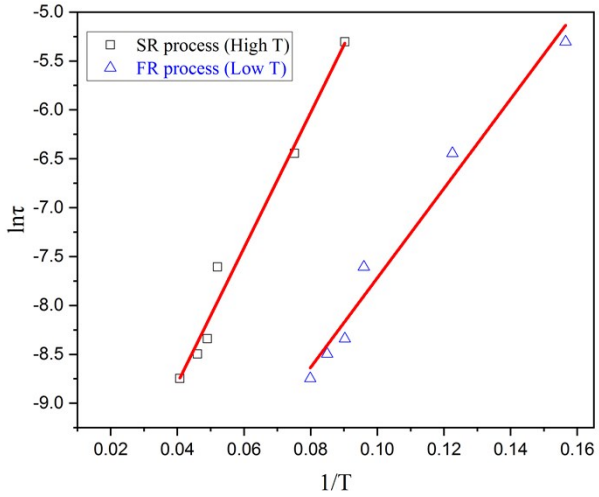

(b)

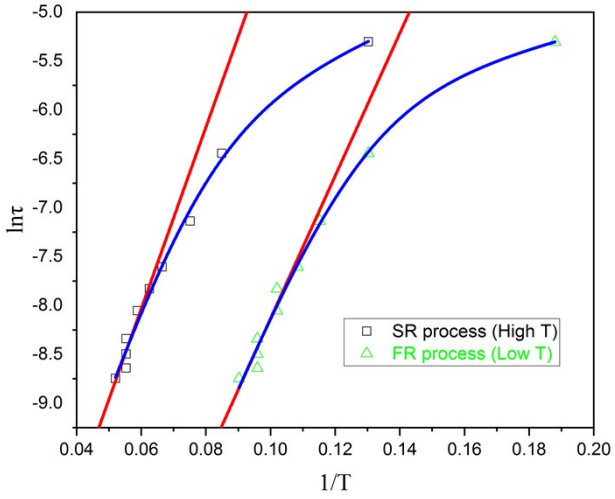

Fig. S6 lnτ vs. T^{-1} plot for 1 (a) and 2 (b) for two relaxation processes; the red solid lines represent the least-squares fits of the experimental data to the Arrhenius law; the blue solid lines are nonlinear fit at low temperature.

Table S7 Some examples of asymmetric dinuclear Dy^{III} SMMs possessing two-step relaxation processes

Complexes	Magnetic behavior	Magnetic Field/ Oe	Energy barrier/ K (Low Temp.)	τ_0/ s (Low Temp.)	Energy barrier/ K (High Temp.)	τ_0/ s (High Temp.)
$[Dy_2(ovph)_2Cl_2(MeOH)_3]\cdot MeCN$[S1]	F	0	150	2.3×10^{-8}	198	7.3×10^{-9}
$[Dy_2(HL)_2Cl_2(H_2O)_3]\cdot 2H_2O\cdot MeCN$[S2]	F	0	103	1.76×10^{-8}	204	5.93×10^{-9}
$[Dy_2(L)_2(acac)_2(H_2O)]\cdot 2CH_2Cl_2$[S3]	F	1500	33.5	6.4×10^{-7}	68.6	1.8×10^{-7}
$[Dy_2(L)_2(DBM)_2(H_2O)]\cdot 2CH_2Cl_2$ [S3]	AF	1500	31.4	6.6×10^{-7}	59.6	7.3×10^{-8}
$[Dy_2(Pc)_2(L\text{-}OCH_3)_2(H_2O)]\cdot 2THF$[S4]	F	0	32.5	3.93×10^{-7}	59.5	1.59×10^{-7}
$[\{Dy(tmh)_3\}_2(\mu_2\text{-}mbpymNO)]\cdot MeOH$[S5]	AF	1000	47.8	$1.5(4) \times 10^{-8}$	54.7	$1.7(3) \times 10^{-6}$
$[Dy_2L_2(HL)(NO_3)(EtOH)]\cdot 0.5(C_2H_5OH)$[this work]	F	0	45.73	4.6×10^{-6}	69.19	9.5×10^{-6}
$[Dy_2L_2(NO_3)(CH_3COO)_2]\cdot Et_3NH$ [this work]	F	0	72.95	2.0×10^{-7}	92.77	1.2×10^{-6}

H-H_2L = 2,2'-(2-hydroxy-3-methoxy-5-methylbenzylazanediyl)diethanol; H_2ovph = ortho-vanillin picolinylhydrazone; H_2-HL = 3- hydroxy-N'-(2-hydroxybenzylidene)picolino hydrazide; H_2L = N,N′- bis(salicylidene)-o-phenylenediamine, acac = acetylacetone, DBM = dibenzoylmethane; H_2Pc = phthalocyanine, HL-OCH3 = 2-hydroxy-3-methoxybenzaldehyde; tmh = 2,2,6,6-tetramethyl-3,5-heptanedionate, mbpymNO = 4-methylbipyrimidine. F = ferromagnetic, AF = antiferromagnetic.

Computational details

Each binuclear complex has two types of Dy^{III} fragments indicated as **1_Dy1, 1_Dy2, 2_Dy1** and **2_Dy2**. Complete-active-space self-consistent field (CASSCF) calculations on individual Dy^{III} fragments (see Fig. S7 for the calculated structures of complexes **1** and **2**) on the basis of single-crystal X-ray determined geometry have been carried out with MOLCAS 8.4[S6] program package. Each individual Dy^{III} fragment in **1** and **2** was calculated keeping the experimentally determined structure of the corresponding compound while replacing the other Dy^{III} ion with diamagnetic Lu^{III}.

The basis sets for all atoms are atomic natural orbitals from the MOLCAS ANO-RCC library: ANO-RCC-VTZP for Dy^{III}; VTZ for close O and N; VDZ for distant atoms. The calculations employed the second order Douglas-Kroll-Hess Hamiltonian, where scalar relativistic contractions were taken into account in the basis set and the spin-orbit couplings were handled separately in the restricted active space state interaction (RASSI-SO) procedure. For individual Dy^{III} fragment, active electrons in 7 active spaces include all *f* electrons (CAS(9 in 7 for Dy^{III})) in the CASSCF calculation. To exclude all the doubts, we calculated all the roots in the active space. We have mixed the maximum number of spin-free state which was possible with our hardware (all from 21 sextets, 128 from 224 quartets, 130 from 490 doublets for Dy^{III}). SINGLE_ANISO[S7] program was used to obtain the energy levels, ***g*** tensors, predominant m_J values, magnetic axes, *et al.,* based on the above CASSCF/RASSI-SO calculations.

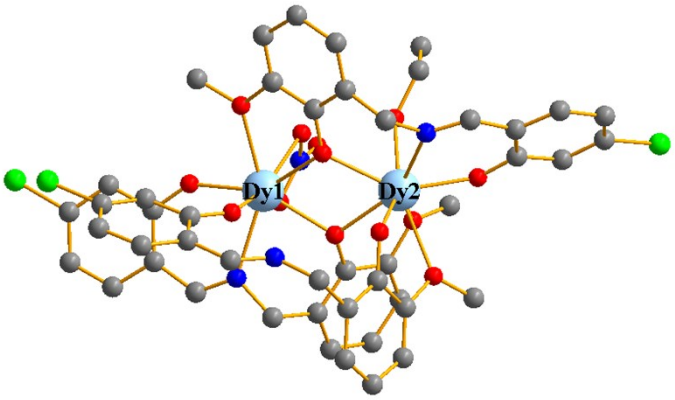

1

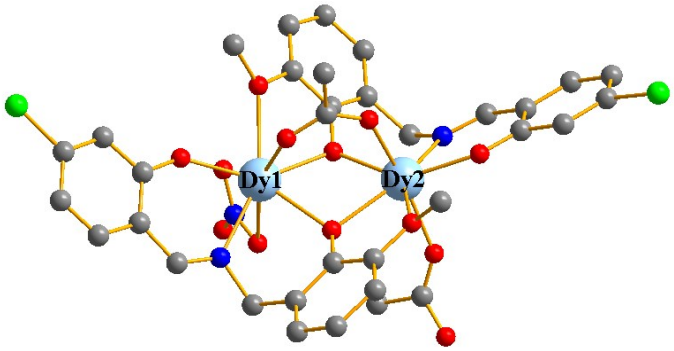

2

Fig. S7 Calculated structures of Dy^{III} fragments in **1** and **2**.

Table S8 Calculated energy levels (cm^{-1}), ***g*** (g_x, g_y, g_z) tensors and predominant m_J values of the lowest eight Kramers doublets (KDs) of individual Dy^{III} fragments for **1** and **2** using CASSCF/RASSI-SO with MOLCAS 8.4

KDs	**1_Dy1**			**1_Dy2**		
	E/cm^{-1}	***g***	m_J	E/cm^{-1}	***g***	m_J
1	0.0	0.003 0.004 19.740	±15/2	0.0	0.012 0.016 19.703	±15/2
2	186.1	0.104 0.125 16.983	±13/2	123.6	0.071 0.092 17.222	±13/2
3	316.0	1.985 6.430 11.313	±7/2	235.6	0.517 0.671 14.331	±11/2
4	348.4	6.987 6.351 2.263	±5/2	329.5	3.383 4.169 10.344	±9/2
5	423.7	3.059 6.616 10.346	±9/2	429.7	3.526 5.095 10.931	±5/2
6	485.6	1.329 3.687 13.379	±3/2	572.0	8.523 6.123 3.097	±3/2
7	549.1	0.877 1.525 17.994	±1/2	618.3	9.798 6.323 2.286	±7/2
8	656.8	0.063 0.150 19.504	±11/2	665.7	0.469 2.072 17.725	±1/2
KDs	**2_Dy1**			**2_Dy2**		
	E/cm^{-1}	***g***	m_J	E/cm^{-1}	***g***	m_J

1	0.0	0.003 0.006 19.694	±15/2	0.0	0.040 0.047 19.630	±15/2
2	195.9	0.219 0.263 16.615	±13/2	91.1	0.212 0.270 19.347	±5/2
3	316.6	2.504 4.088 13.650	±7/2	180.9	0.582 0.961 16.329	±13/2
4	368.8	1.499 4.956 8.499	±11/2	264.7	2.667 3.593 14.045	±11/2
5	447.4	9.231 7.014 4.139	±9/2	345.5	8.755 7.069 2.337	±9/2
6	477.4	0.998 1.678 17.418	±3/2	441.7	2.249 3.177 14.223	±1/2
7	545.4	0.540 0.845 18.409	±1/2	574.3	0.978 1.716 16.156	±3/2
8	606.9	0.155 0.402 19.331	±5/2	610.7	0.528 2.885 17.254	±7/2

Table S9 Wave functions with definite projection of the total moment | m_J > for the lowest two KDs of individual Dy^{III} fragments for **1** and **2** using CASSCF/RASSI-SO with MOLCAS 8.4

	E/cm^{-1}	wave functions
1_Dy1	0.0	98%|±15/2>
	186.1	90%|±13/2>
1_Dy2	0.0	98%|±15/2>
	123.6	82%|±13/2>+10%|±11/2>
2_Dy1	0.0	97%|±15/2>
	195.9	92%|±13/2>
2_Dy2	0.0	97%|±15/2>
	91.1	14%|±7/2>+21%|±5/2>+25%|±3/2>+27%|±1/2>

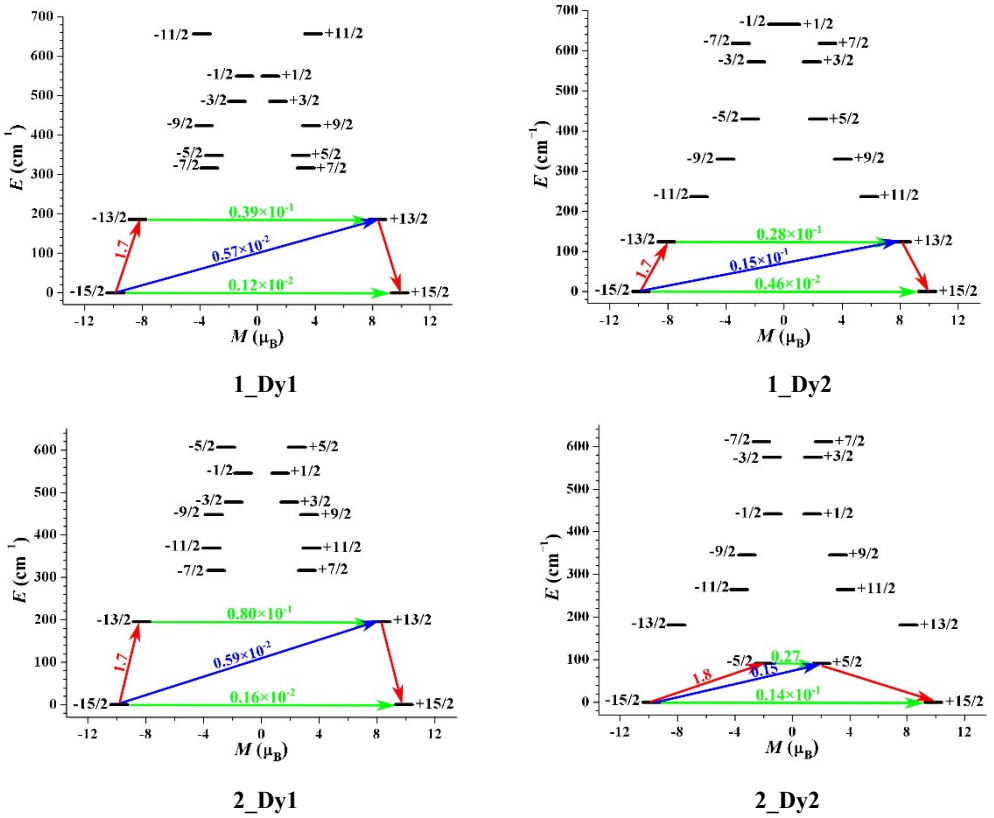

Fig. S8 Magnetization blocking barriers for individual Dy^{III} fragments in **1** and **2**. The thick black lines represent the KDs of the individual Dy^{III} fragments as a function of their magnetic moment along the magnetic axis. The green lines correspond to diagonal matrix element of the transversal magnetic moment; the blue line represent Orbach relaxation processes. The path shown by the red arrows represents the most probable path for magnetic relaxation in the corresponding compounds. The numbers at each arrow stand for the mean absolute value of the corresponding matrix element of transition magnetic moment.

To fit the exchange interactions between Dy^{III} ions in complexes **1** and **2**, we took two steps to obtain them. Firstly, we calculated individual Dy^{III} fragment using CASSCF/RASSI-SO to obtain the corresponding magnetic properties. Then, the exchange interactions between the magnetic centers are considered within the Lines model,[S8] while the accounts of the dipole-dipole magnetic couplings are treated exactly. The Lines model is effective and has been successfully used widely in the research field of *d* and *f*-elements single-molecule magnets.[S9]

The Ising exchange Hamiltonians is:

$$H_{exch} = -JS_{Dy1}S_{Dy2} \quad (1)$$

The total J_{total} is the parameter of the total magnetic interaction ($J_{total} = J_{dipolar} + J_{exchange}$) magnetic center ions. The S_{Dy} = 1/2 is the ground pseudospin on the Dy^{III} site. The dipolar magnetic coupling can be calculated exactly, while the exchange coupling constant was fitted through comparison of the computed and measured magnetic susceptibilities using the POLY_ANISO program.[S8]

Table S10 Exchange energies E (cm^{-1}), the energy difference between each exchange doublets Δ_t (cm^{-1}) and the main values of the g_z for the lowest two exchange doublets of **1** and **2**

	1			**2**		
	E	Δ_t	g_z	E	Δ_t	g_z
1	0.0	5.75×10^{-8}	38.215	0.0	1.11×10^{-6}	38.192
2	2.6	4.99×10^{-7}	9.780	1.9	3.48×10^{-6}	9.361

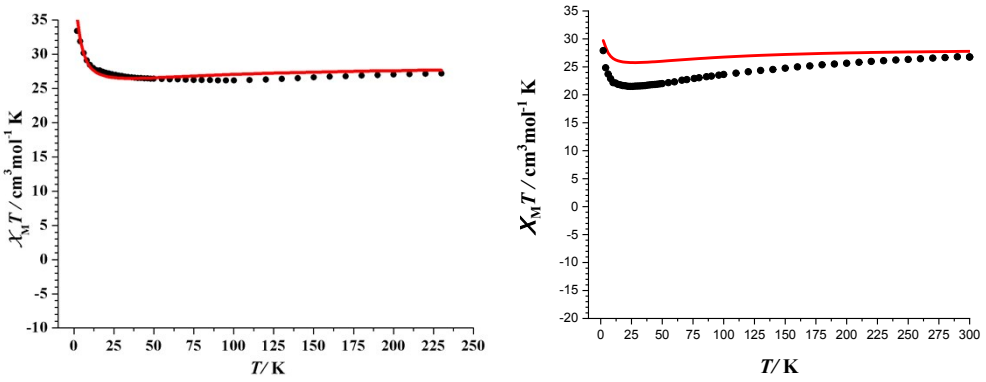

Fig. S9 Calculated (red solid line) and experimental (black circle dot) data of magnetic susceptibilities of **1** and **2**. The intermolecular interactions zJ' of **1** and **2** were fitted to −0.01 and −0.02 cm^{-1}, respectively.

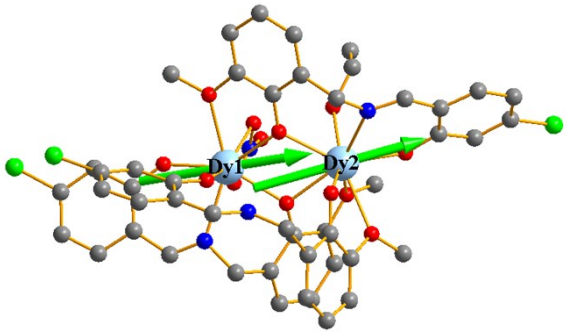

1

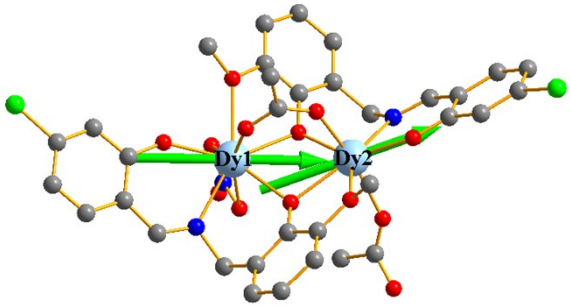

2

Fig. S10 Calculated orientations of the local main magnetic axes on Dy^{III} ions of complexes **1** and **2** in the ground KDs.

References:

S1 Y. N. Guo, G. F. Xu, W. Wernsdorfer, L. Ungur, Y. Guo, J. Tang, H. J. Zhang, L. F. Chibotaru, and A. K. Powell, *J. Am. Chem. Soc.,* 2011, **133**, 11948.

S2 L. Zhang, J. Jung, P. Zhang, M. Guo, J. K. Tang and B. L. Guennic, *Chem. Eur. J.,* 2016, **22**, 1392.

S3 W. Y. Zhang, P. Chen, Y. M. Tian, H. F. Li, W. B. Sun and P. F. Yan, *CrystEngComm,* 2018, **20**, 777.

S4 J. Y. Ge, H. Y. Wang, J. Su, J. Li, B. L. Wang, Y. Q. Zhang and J. L. Zuo, *Inorg. Chem.,* 2018, **57**, 1408.

S5 I. F. Díaz-Ortega, J. M. Herrera, D. Aravena, E. Ruiz, T. Gupta, G. Rajaraman, H. Nojiri and E. Colacio, *Inorg. Chem.,* 2018, **57**, 6362.

S6 F. Aquilante, J. Autschbach, R. K. Carlson, L. F. Chibotaru, M. G. Delcey, L. De Vico, I. Fdez. Galván, N. Ferré, L. M. Frutos, L. Gagliardi, M. Garavelli, A. Giussani, C. E. Hoyer, G. Li Manni, H. Lischka, D. Ma, P. Å. Malmqvist, T.

Müller, A. Nenov, M. Olivucci, T. B. Pedersen, D. Peng, F. Plasser, B. Pritchard, M. Reiher, I. Rivalta, I. Schapiro, J. Segarra‐Martí, M. Stenrup, D. G. Truhlar, L. Ungur, A. Valentini, S. Vancoillie, V. Veryazov, V. P. Vysotskiy, O. Weingart, F. Zapata, R. Lindh, MOLCAS 8: New Capabilities for Multiconfigurational Quantum Chemical Calculations across the Periodic Table. *J. Comput. Chem*., 2016, **37**, 506.

S7 (a) Chibotaru, L. F.; Ungur, L.; Soncini, A. *Angew. Chem. Int. Ed.,* 2008, **47**, 4126. (b) Ungur, L.; Van den Heuvel, W.; Chibotaru, L. F. *New J. Chem.,* 2009, **33**, 1224. (c) Chibotaru, L. F.; Ungur, L.; Aronica, C.; Elmoll, H.; Pilet, G.; Luneau, D. *J. Am. Chem. Soc.,* 2008, **130**, 12445.

S8 Lines, M. E. *J. Chem. Phys*., 1971, **55**, 2977.

S9 (a) Mondal, K. C.; Sundt, A.; Lan, Y. H.; Kostakis, G. E.; Waldmann, O.; Ungur, L.; Chibotaru, L. F.; Anson, C. E.; Powell, A. K. *Angew. Chem. Int. Ed*., 2012, **51**, 7550. (b) Langley, S. K.; Wielechowski, D. P.; Vieru, V.; Chilton, N. F.; Moubaraki, B.; Abrahams, B. F.; Chibotaru, L. F.; Murray, K. S. *Angew. Chem. Int. Ed*., 2013, **52**, 12014.